Cryogenic characterization of the grating vector APP coronagraph for the upcoming ERIS instrument at the VLT

Anna Boehle[a], Adrian M. Glauser[a], Matthew A. Kenworthy[b], Frans Snik[b], David Doelman[b], Sascha P. Quanz[a], and Michael R. Meyer[c]

[a]Institute for Particle Physics and Astrophysics, ETH Zurich, Zurich, Switzerland
[b]Leiden Observatory, Leiden University, Leiden, Netherlands
[c]Department of Astronomy, University of Michigan, Ann Arbor, USA

ABSTRACT

We present results from a cryogenic characterization of the grating vector Apodizing Phase Plate (gvAPP) coronagraph that will be used in the upcoming instrument ERIS (Enhanced Resolution Imager and Spectrograph) at the VLT. ERIS consists of a 1-5 μm imager (NIX) and a 1−2.5 μm integral field spectrograph (SPIFFIER), both fed by the Adaptive Optics Facility of UT4 to yield diffraction-limited spatial resolution. A gvAPP coronagraph will be included in the NIX imager to enable high-contrast imaging observations, which will be particularly powerful for the direct imaging of exoplanets at L and M bands (∼3−5 μm) and will compliment the current capabilities of VLT/SPHERE and surpass the capabilities of VLT/NACO. We utilize the near-infrared test bench of the Star and Planet Formation group at ETH Zurich to measure key properties of the gvAPP coronagraph at its operating wavelengths and under the vacuum/cryogenic (∼70 K) conditions of the future ERIS instrument.

Keywords: VLT, ERIS, coronagraphy, direct imaging of exoplanets, high contrast imaging, grating vector APP, Apodizing Phase Plate coronagraph, APP

1. INTRODUCTION

High contrast imaging of exoplanets is as a powerful technique for constraining the occurrence rate of gas giant exoplanets at wide separations and for characterizing giant exoplanet atmospheres (e.g., Ref. 1). This direct detection technique requires high angular resolution to spatially resolve the planet and the star as well as hardware and software techniques to suppress and subtract the light from the central star to reveal the much fainter exoplanet. Direct imaging observations are typically performed at near-infrared (NIR; 1−5 μm) wavelengths where the thermal emission of the exoplanets can be detected. High contrast imaging at the longer NIR wavelengths (3−5 μm, L′/M′ bands) is complimentary to the 1−2.5 μm imaging performed by extreme adaptive optics instruments such as VLT/SPHERE and Gemini/GPI because - in principle - the longer wavelengths are sensitive to cooler and therefore older/less-massive planets.

The upcoming ERIS (Enhanced Resolution Imager and Spectrograph)[2] instrument will greatly improve the 3 - 5 μm high contrast imaging capabilities at the European Southern Observatory Very Large Telescope (VLT). ERIS includes both a 1−5 μm imager (NIX[3]) and a 1−2.5 μm integral field spectrograph (SPIFFIER[4]). Both NIX and SPIFFIER will be fed by the ERIS AO module,[5] which uses the deformable secondary mirror of the Adaptive Optics Facility (AOF) on Unit Telescope 4 (UT4) for wavefront correction. By coupling NIX with the deformable secondary mirror, the number of warm reflections prior to the instrument cryostat and therefore the instrumental thermal background will be significantly reduced compared to the current 1−5 μm imager VLT/NACO, making NIX a particularly powerful instrument for high contrast imaging of exoplanets at the longer NIR wavelengths.

NIX will be equipped with a grating vector Apodizing Phase Plate (gvAPP) coronagraph as well as an Annular Groove Phase Mask (AGPM) vortex coronagraph to improve the detection of faint exoplanet companions.[6] APP coronagraphs operate in the pupil plane and are thus insensitive to residual tip/tilt variations, in contrast to

Send correspondence to A.B.:
E-mail: boehlea@phys.ethz.ch, Telephone: +41 (0)44 632 09 56

focal plane coronagraphs such as vortex coronagraphs and the traditional Lyot stop. A disadvantage of previous APP designs is that they carve out an asymmetric, D-shaped dark region on only one side of the central star, necessitating two observations of the same star with a 180 degree rotation to search for planets at all azimuths. The gvAPP solves this issue by splitting the left and right circular polarizations of the light to simultaneously produce two images of the star with a D-shaped dark region on either side.[7,8] Figure 1 shows the theoretical point spread function (PSF) of the ERIS gvAPP, which was designed at Leiden Observatory and manufactured by ImagineOptix. This coronagraph is envisioned to operate in NIX in the L′ ($\lambda_o = 3.8\mu$m, $\Delta\lambda = 0.6$ μm) and M′ bands ($\lambda_o = 4.8\mu$m, $\Delta\lambda = 0.6\mu$m), although the achromatic nature of the gvAPP design also allows it to operate at shorter wavelengths.

In this work, we characterize the ERIS gvAPP under the cryogenic conditions of the future instrument and at its operating wavelengths. Laboratory characterizations of coronagraphs are typically performed at room temperature, limiting the characterizations to wavelengths shorter than 2 - 2.5 μm due to the high thermal background at longer infrared wavelengths. Here we employ the cryogenic NIR test bench of the Star and Planet Formation group at ETH Zurich[9] to produce diffraction-limited images of the ERIS gvAPP PSF at the L′ band wavelength of 3.8 μm. These measurements will serve as a key comparison between the theoretically predicted gvAPP PSF and the on-sky PSF that will be observed when ERIS is commissioned at the VLT in 2020. Below we summarize the capabilities of the ETH Zurich cryogenic NIR test bench and the experimental setup for measuring the ERIS gvAPP PSF (Sec. 2) and present results on the coronagraph performance including the PSF morphology, overall throughput, and relative intensity as a function of separation (Sec. 3).

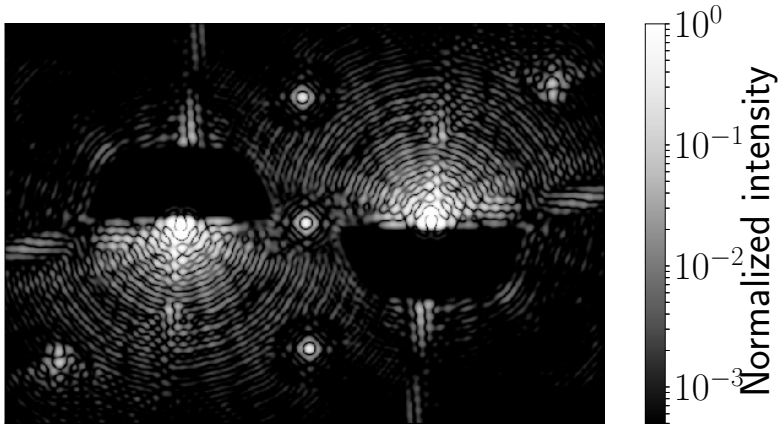

Figure 1. Theoretical PSF of the ERIS gvAPP. The gvAPP produces two main images from a single point source, each with a D-shaped dark region on either side of the central point source. This coronagraph therefore allows both sides of a star to be probed for faint companions simultaneously, a significant advantage over previous APP designs. The PSF components between the two main images, of which the central one is the brightest, serve as astrometric and photometric references.

2. gvAPP PSF MEASUREMENTS USING THE ETH ZURICH CRYOGENIC NEAR-INFRARED TEST BENCH

Measurements of the ERIS gvAPP PSF were performed using the ETH Zurich[9] cryogenic NIR test bench (Fig. 2). This test bench is designed to test focal plane, pupil plane, and spectrally dispersive optics from $1 - 5$ μm under cryogenic ($\sim$70 K) conditions. The optical design of the bench uses 4 off-axis parabolic mirrors to generate two intermediate pupil planes and one intermediate focal plane between the two collimated spaces. The test bench is based around an engineering-grade, 5 μm-cutoff Hawaii-2RG detector from Teledyne that is housed in a separate cryostat made by GL Scientific (GLS). The interface between the optical bench cryostat and the GLS detector

Figure 2. Image of the ETH Zurich cryogenic near-infrared test bench. The test bench is based around a 5 μm-cutoff Teledyne Hawaii-2RG detector and allows for the characterization of focal plane, pupil plane, and dispersive optical components under vacuum/cryogenic ($\sim$70 K) conditions.

cryostat includes a gate valve so that the two cryostats can be operated completely independently. The test bench had first light in 2012 and achieves diffraction-limited performance across its operating wavelengths.

In early 2018, the test bench was upgraded to include a short-pass filter with the goal of reducing excess thermal background. The selected short pass filter blocks light beyond 4.5 μm and was purchased from Spectrogon. The filter is installed inside the GLS cryostat at the end of the final detector baffle (Fig. 3) to maximize the amount of blocked thermal background from the optical bench cryostat. For a 180 K blackbody (the temperature of the radiation shield in the optical bench cryostat), the short pass filter blocks out $\sim$90% of the thermal background light in the 1 - 5.4 μm sensitivity range of the detector. The short pass filter slightly vignettes the optical beam, resulting in a smaller but still sufficient field of view for these and other measurements.

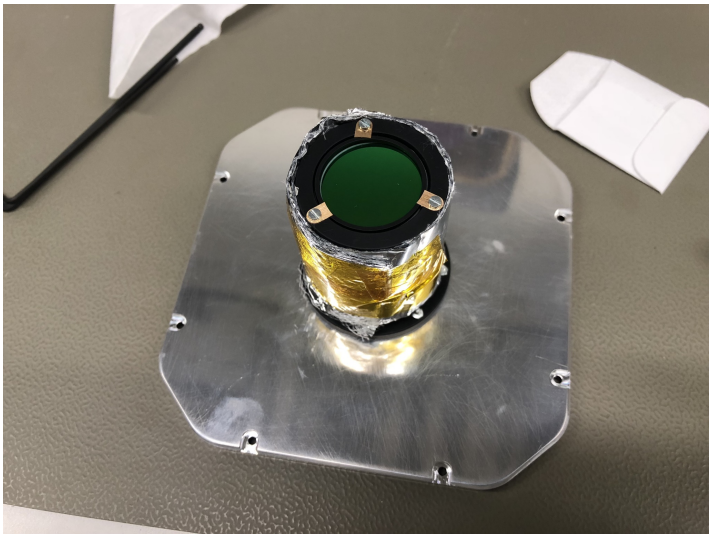

Figure 3. Short pass filter installed in the final baffle before the Hawaii-2RG detector. The filter was purchased from Spectrogon and blocks light with a wavelength longer than 4.5μm to reduce the excess thermal background.

We measure the PSF of the ERIS gvAPP and compare it with a measured PSF produced by a VLT pupil mask. Comparing to a VLT pupil mask PSF is necessary because the gvAPP itself includes a VLT pupil mask, used to block out emission from the UT4 secondary mirror spiders and baffle. Figure 4 shows both the ERIS gvAPP and the VLT pupil mask installed in the first filter wheel of the second pupil plane in the ETH Zurich cryogenic NIR test bench. To measure the PSFs of the gvAPP and the VLT pupil mask, a point source is created using the tungsten light source installed prior to the entrance window of the bench cryostat and a 30 μm pinhole mask in the intermediate focal plane. All measurements presented here were taken using a 3.8 μm filter with a 5% bandpass installed in the second filter wheel of the second pupil plane. This filter is the closest filter in the test bench to the standard L$'$ filter, with the same central wavelength as L$'$ and one third of the total bandpass.

The field of view of the test bench that is not affected by vignetting is too small to fit the left and right gvAPP PSFs simultaneously, so measurements of each PSF component were taken separately. For the measurements of each PSF component the tip/tilt of the final fold mirror before the GLS detector cryostat was adjusted to move that component to near the center of the unvignetted field of view. The detector was read out in a subarray centered on the peak of the PSF, with the size of the subarray chosen such that the central pixels of the PSF remained in the linear detector regime for at least the first two reads. The left, right, and central (i.e., the brightest of the 3 middle PSF components; see Fig. 1) gvAPP PSF components were each measured in a 200 by 200 pixel subarray with a readout time of 0.42 sec. Due to the higher overall throughput of the VLT pupil mask compared to the gvAPP, a smaller window of 90 by 90 pixels with a readout time of 0.09 sec was required to avoid immediate saturation of the central pixels. The gvAPP and VLT pupil mask PSFs were measured using an up-the-ramp readout scheme with 20 and 100 reads respectively and 20 total ramps. An image was created from each ramp by fitting a line to the detector reads, excluding all reads where the detector is in the non-linear regime, and then all individual frames were averaged. For each PSF measurement, background measurements were also taken with the same readout scheme with the first filter wheel in the test bench system set to the blank position to subtract from the PSF images. To correct for bad pixels, this full procedure was repeated 3 times for each PSF after dithering the position of the PSF a few pixels by finely adjusting the x/y position of the GLS detector cryostat perpendicular to the optical axis. Each of the 3 dithered positions were flagged for bad pixels and then median combined. With the 20 and 100 ramps of the gvAPP and VLT pupil mask measurements and the 3 dithered positions, the final measurements of each PSF have a total of 25 and 27 min of integration time respectively. For all measurements, the cryocoolers of both the optical bench and detector cryostats were switched off to eliminate any vibrations that would affect the shape of the measured PSFs.

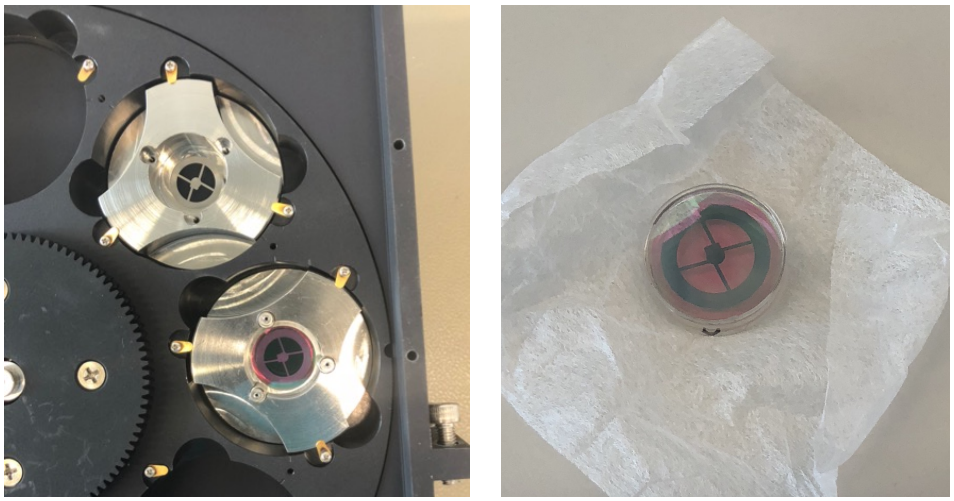

Figure 4. Left: image of the VLT pupil mask (top) and the ERIS gvAPP (bottom) installed in the first filter wheel of the second pupil plane in the ETH Zurich cryogenic near-infrared test bench. Right: close up view of the gvAPP coronagraph. The VLT pupil mask is identical to the pupil mask included in the gvAPP and is used to produce a nominal PSF to compare with the PSF of the gvAPP. For reference, the VLT pupil mask is 11.3 mm (0.45 inches) in diameter.

3. ANALYSIS AND RESULTS: CHARACTERIZATION OF THE ERIS gvAPP PSF

The final left and right gvAPP PSF images along with the VLT pupil mask PSF image for comparison are shown in Fig. 5. We find that the morphology of the gvAPP PSFs are comparable to the theoretical predictions for the gvAPP design. We detect faint structures in the gvAPP PSF across the field of view of the measurements (14 λ/D on a side). The measured gvAPP is elongated in comparison to the theoretical predictions as expected given that the measurements are across a 5% wavelength bandpass and the predictions are at a single wavelength.

We further characterize the ERIS gvAPP by measuring the overall throughput of the coronagraph. We first sum the background-subtracted counts in the full field of view of the final left, center, and right gvAPP PSF images. The background for each image is determined using a circular apertures in the dark regions of the gvAPP PSFs with radii of 10 pixels. The total counts contained in all 3 gvAPP PSF components is then compared to the background-subtracted counts summed over the full field of view of the VLT pupil mask. The VLT pupil mask background is determined by placing 4 small circular apertures with radii of 2 pixels at dark locations in the PSF. The ratio of the total counts in the gvAPP and the VLT pupil mask PSFs then determines the overall throughput of the coronagraph. Since the field of view of the VLT pupil mask PSF image is smaller than that of the gvAPP image, this ratio produces an upper limit on the overall throughput. A lower limit is also placed by comparing the gvAPP counts only in the smaller region also covered by the VLT pupil mask image. From these ratios, we find that the overall throughput of the gvAPP coronagraph is 60 to 70%, which is consistent with the theoretical predictions from the design of the ERIS gvAPP coronagraph.

We also measure the amount of light contained in the cores of the left/right gvAPP PSFs. The total light in the core is affected by the overall throughput of the gvAPP, the splitting of the right/left circularly polarized light to create the two PSFs with a dark region on either side, and the modified shape of each gvAPP PSF compared to VLT pupil mask PSF. To measure the number of counts in the core of each PSF, we sum the counts in a circular aperture on the core of the PSF with a radius of 13.9 pixels, corresponding to the diffraction limit for a 11.3 mm pupil at 3.8 μm. The background is subtracted from the total counts in the aperture using the same background determined previously for the throughput measurement. The same measurement is performed on each of the gvAPP PSFs and the VLT pupil mask PSF. We find that the cores of the right and left gvAPP PSFs individually contain approximately 20% of the counts in the core of the VLT PSF. This value corresponds to 27% - 33% of the counts in the VLT PSF core after correcting for the overall throughput of the coronagraph. Combining the throughput-corrected counts in the left and right gvAPP PSFs yields 55% - 64% of the counts in the VLT PSF core, consistent with theoretical predictions.

The gvAPP and VLT pupil mask PSFs are also compared quantitatively by plotting the profiles of the PSFs, shown in Fig. 6. We compare the profile of the gvAPP PSFs in their respective dark regions and the azimuthally averaged profile of the VLT pupil mask PSF. In both cases, the PSF profiles at a given separation are measured by averaging the total counts in a set of circular apertures evenly spaced in angle across the azimuth range of interest. A small azimuth range of 60 degrees is taken for the gvAPP dark region profiles, set by the angles at which the dark region begins approximately 1 resolution element away from the center of the PSF core. The PSF profiles are then background subtracted, and any values that are within 1-sigma of the background are taken to be at the background limit and are not plotted in Fig. 6. We find that at separations > 2.0 λ/D the intensity of the dark region of each gvAPP PSF is $<1.5 \times 10^{-3}$ relative to its peak intensity. PSF profile measurements beyond this separation are at the background limit of the bench and so we report an upper limit of the depth of the gvAPP dark region. We are currently exploring ways to improve this lower limit by reducing the residual thermal background and/or by increasing the intensity of the light source relative to the background.

The images of both the left and right gvAPP PSFs show an additional image of the PSF that is offset and rotated with respect to the PSF and is likely a ghost image. Further tests are necessary to determine the origin of these ghost images. The ghost may be created by reflections within the test bench, most likely coming from the photometric filter or the short pass filter. Another possibility is that there was a mistake in the manufacturing of the gvAPP and the ghost comes from layers within the coronagraph itself. The manufacturer also delivered a second gvAPP coronagraph that we will characterize with the test bench, which will help to determine the source of the ghost images seen in these data.

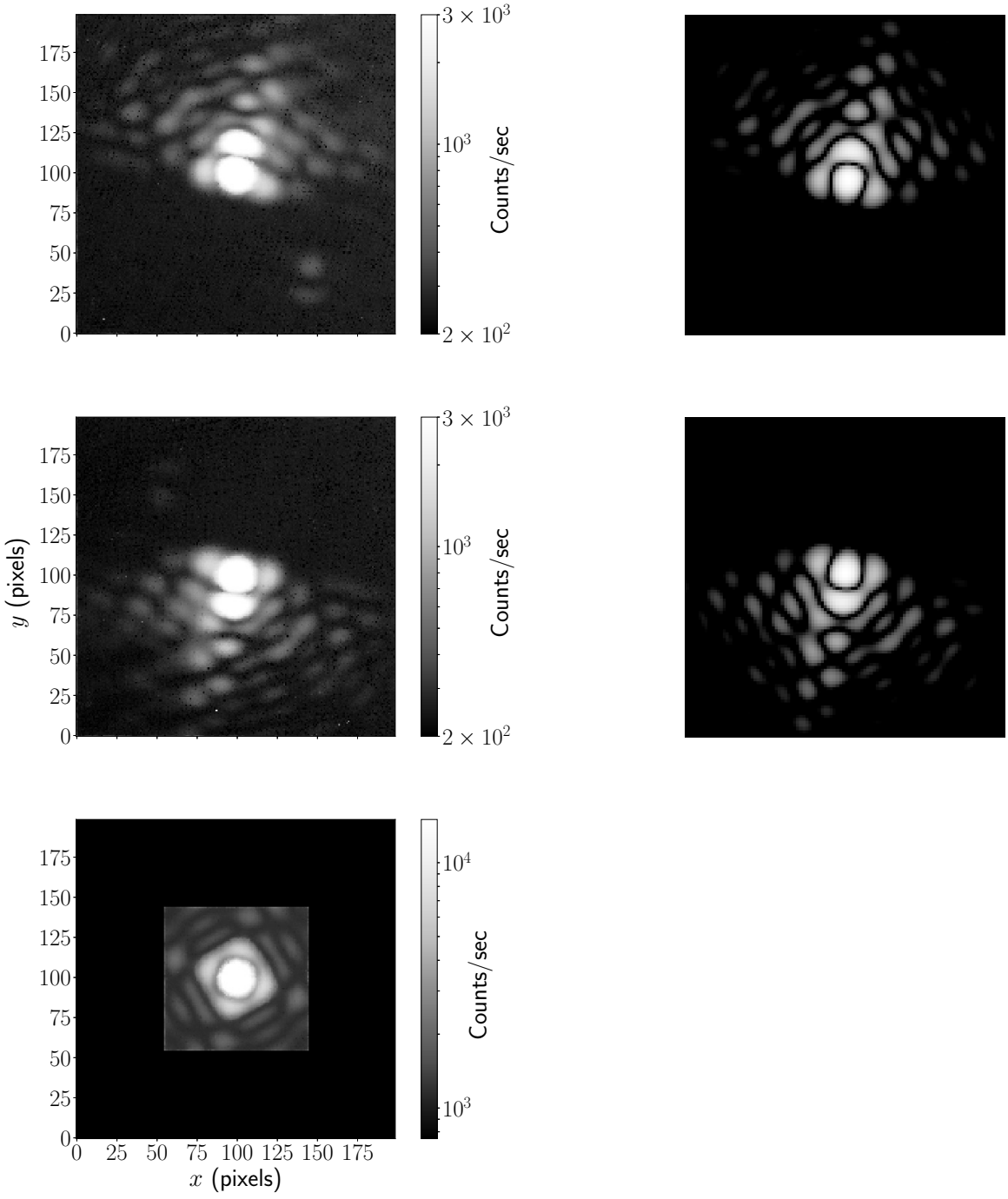

Figure 5. Final images of the gvAPP (top and middle left) and VLT pupil mask (bottom left) PSFs measured with the ETH Zurich cryogenic near-infrared test bench. We find that the gvAPP PSF morphology is comparable to the theoretical predictions (top and middle right). The predictions plotted here are subsets of the same theoretical PSF shown in Fig. 1, with the PSF rotated and the color bar scaled to match the measurements.

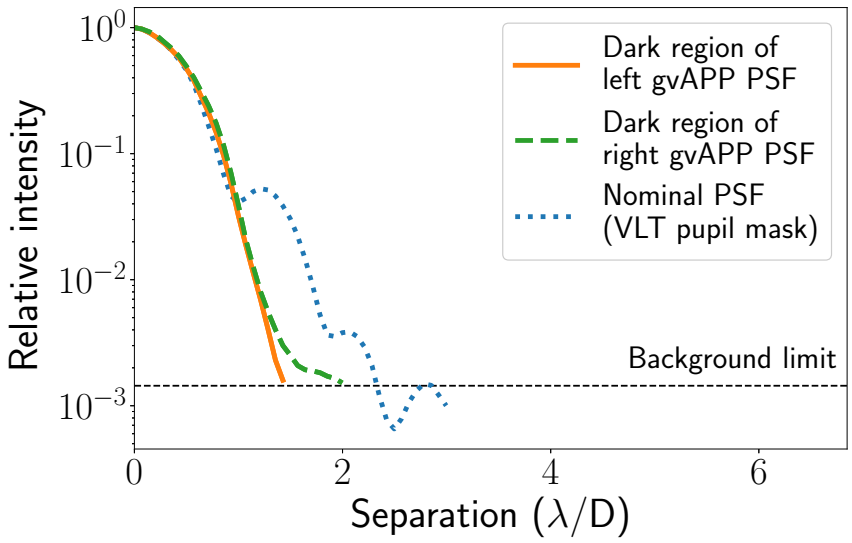

Figure 6. gvAPP and VLT pupil mask PSF profiles with the residual background subtracted and normalized to their peak intensity. The VLT profile is averaged over all azimuths and the gvAPP profiles are measured across a 60 degree range within the dark regions. Profile values consistent with the residual background are shown as the 1-σ background limit. Note that the VLT pupil mask profile stops at $\sim$3 λ/D due to the smaller field of view of this PSF image.

4. SUMMARY

The NIX imager in the upcoming ERIS instrument at the VLT will greatly improve upon the current 1−5 μm imaging capabilities of VLT/NACO and its high contrast imaging of exoplanets at 3−5 μm will compliment instruments such as VLT/SPHERE. Here we use the ETH Zurich cryogenic NIR test bench to characterize the ERIS gvAPP coronagraph under the operating conditions of the future instrument and at its operating wavelengths of 3.8 μm. We find that the morphology, overall throughput, and core intensity of the gvAPP PSF compared with a nominal VLT PSF is consistent with the theoretical predictions. We place an upper limit on the PSF intensity in the dark regions of $<1.5 \times 10^{-3}$ relative to the peak intensity of the gvAPP PSF at separations > 2.0 λ/D. This upper limit is set by the background limit of the test bench at 3.8 μm, and we are exploring options to improve this limit by reducing the thermal background and/or increasing the intensity of the PSF relative to the background.

REFERENCES

[1] Bowler, B. P., "Imaging Extrasolar Giant Planets," *Publications of the Astronomical Society of the Pacific* **128**, 102001 (Oct. 2016).

[2] Davies, R., Esposito, S., Feuchtgruber, H., Kenworthy, M. A., Schmid, H. M., Sturm, E., and Taylor, W. D., "ERIS: revitalising an adaptive optics instrument for the VLT," in [*Ground-based and Airborne Instrumentation for Astronomy VII*], Proc. SPIE **10702**, Paper 8 (2018).

[3] Pearson, D., Taylor, W., Davies, R., MacIntosh, M., Henry, D., Lunney, D., Waring, C., Gao, X., Lightfoot, J., Glauser, A. M., Quanz, S. P., Meyer, M. R., Schmid, H. M., March, S., Bachmann, W., Feuchtgruber, H., George, E., Sturm, E., Biller, B., Hinckley, S., Kenworthy, M., Amico, P., Glindemann, A., Kasper, M., Kuntschner, H., Dorn, R., and Egner, S., "NIX, the imager for ERIS: the AO instrument for the VLT," in [*Ground-based and Airborne Instrumentation for Astronomy VI*], **9908**, 99083F (Aug. 2016).

[4] George, E. M., Gräff, D., Feuchtgruber, H., Hartl, M., Eisenhauer, F., Buron, A., Davies, R., Genzel, R., Huber, H., Rau, C., Plattner, M., Wiezorrek, E., Weisz, H., Amico, P., Glindemann, A., Hau, G., and Kuntschner, H., "Making SPIFFI SPIFFIER: upgrade of the SPIFFI instrument for use in ERIS and

performance analysis from re-commissioning," in [*Ground-based and Airborne Instrumentation for Astronomy VI*], **9908**, 99080G (Aug. 2016).

[5] Riccardi, A., Esposito, S., Agapito, G., Antichi, J., Biliotti, V., Blain, C., Briguglio, R., Busoni, L., Carbonaro, L., Di Rico, G., Giordano, C., Pinna, E., Puglisi, A., Spanò, P., Xompero, M., Baruffolo, A., Kasper, M., Egner, S., Suàrez Valles, M., Soenke, C., Downing, M., and Reyes, J., "The ERIS adaptive optics system," in [*Adaptive Optics Systems V*], **9909**, 99091B (July 2016).

[6] Kenworthy, M. A., Snik, F., Keller, C. U., Doelman, D., Por, E. H., Absil, O., Carlomagno, B., Karlsson, M., Huby, E., Glauser, A. M., Quanz, S. P., and Taylor, W. D., "High contrast imaging for the enhanced resolution imager and spectrometer (ERIS) ," in [*Ground-based and Airborne Instrumentation for Astronomy VII*], Proc. SPIE **10702**, Paper 151 (2018).

[7] Snik, F., Otten, G., Kenworthy, M., Miskiewicz, M., Escuti, M., Packham, C., and Codona, J., "The vector-APP: a broadband apodizing phase plate that yields complementary PSFs," in [*Modern Technologies in Space- and Ground-based Telescopes and Instrumentation II*], **8450**, 84500M (Sept. 2012).

[8] Otten, G. P. P. L., Snik, F., Kenworthy, M. A., Miskiewicz, M. N., and Escuti, M. J., "Performance characterization of a broadband vector Apodizing Phase Plate coronagraph," *Optics Express* **22**, 30287 (Dec. 2014).

[9] Wehmeier, U. J., Leisenring, J., Durney, O., Solheid, E., Luppino, G. A., and Meyer, M. R., "An integrated 1-5 micron test bench for the characterization of cryogenic optical elements," in [*Ground-based and Airborne Instrumentation for Astronomy IV*], **8446**, 84463G (Sept. 2012).